Pergamon

Int. J. Heat Mass Transfer. Vol. 40, No. 3, pp. 727–735, 1997
Copyright © 1996 Elsevier Science Ltd
Printed in Great Britain. All rights reserved
0017-9310/97 $15.00+0.00

PII: S0017-9310(96)00132-9

Mass transfer by simultaneous dropwise condensation and particle deposition

M. J. TIERNEY and G. L. QUARINI
University of Bristol, Bristol BS8 1TR, U.K.

(*Received* 4 *August* 1994 *and in final form* 27 *March* 1995)

Abstract—Measurements have been made of the deposition rates of water droplets, typically 20 μm in diameter, from an air stream. A number of mass transfer processes can be postulated, including condensation and the turbulent deposition of particles, but in addition we can estimate the influence of thermophoresis and diffusiophoresis on the movement of droplets through boundary layers. We first show rates of particle transport under adiabatic conditions, in which turbulence mechanisms prevail. These are at the upper limit of the wide range of results reported in the previous literature. We believe turbulence may well have been enhanced due to distortions in the test-section shape, necessary for the installation of instrumentation. Deposition rates are increased significantly in the presence of condensation. A phenomenological model, accounting for the influence of thermo- and diffusiophoresis, underpredicts the additional particle deposition. Given observations of dropwise condensation, the associated roughening of the walls is thought to be responsible for the discrepancy, and is identified as an area for further development.
Copyright © 1996 Elsevier Science Ltd.

INTRODUCTION

This paper relates to the study of the deposition rates of water from a water–air aerosol onto the walls of a pipe. The influence of (1) air turbulence and (2) the processes associated with condensation were of interest. Thus the aerosol was transported within a humid carrier gas, the test-section sides could be either cooled or made adiabatic.

There are several studies of turbulence induced deposition in tubular ducts, under adiabatic conditions. However, Hanratty and McCoy's review [1] shows large differences between the results of different workers. When made non-dimensional, the reported deposition rates vary by as much as a factor of 100.

Three deposition regimes have been identified [2, 3]. The 'diffusion dominated regime' applies to submicron sized particles. Their motion through the turbulent boundary layer is considered as Brownian. In the 'eddy diffusivity-impaction regime' a particle enters the turbulent boundary later from the bulk gas, and is assumed to travel part of the way to the wall under the influence of turbulence. However, it retains a significant amount of momentum, whereas close to the wall the eddy diffusivity is relatively small. Hence the final portion of the trajectory is said to be completed by 'free flight'. This regime would typically apply to a size range of between 1 and 10 μm. Finally, in the 'impaction regime' particles are accelerated by turbulence in the bulk of the gas stream, such that they have sufficient inertia to pass through the boundary layer without undergoing a significant change in velocity.

In practice, many engineering geometries are more complex than a simple tube—for instance there is recent interest in spray driers [4] and chemical vapour deposition [5].

A more longstanding concern has been in fast reactor systems [6], where natural convection currents can transport sodium-argon aerosols into the expansion gaps surrounding pumps and heat exchangers. In the latter case condensation and particle deposition occur simultaneously. A tube shape was chosen for our own experiments, because significant data for turbulence induced particle transport were already available.

APPARATUS

A flowsheet of the apparatus is provided in Fig. 1. Three features can be identified: treatment of the air supply, the test-section itself and the associated instrumentation. Pretreatment was required to ensure a supply of up to 3000 Nl min^{-1} of air, at temperatures between -40°C and $+45$°C and relative humidities between 0 and 100%. Air at 6 bar was taken from a ring main and dried to a dew point of -70°C by a proprietary pressure swing adsorption system (manufacturer Pall U.K. Ltd). The supply could be cooled by a heat exchanger/two stage refrigeration assembly, and then heated electrically to within 0.5°C of a set-point. Moisture could be added in a column containing a packed bed plus integral water supply.

The supply was passed through an aerosol generator (Fig. 2). A portion of the air supply was compressed to approximately 3 bar and passed through a nozzle, drawing in water from either an integral reservoir or a graduated sight tube. The aerosol then

NOMENCLATURE

A	surface area of the test-section
C	mass concentration of aerosol particles
C_v	vapour concentration
d_g	geometric mean diameter
d_m	mean diameter on basis of particle mass
d_p	particle diameter
D	diameter of the test-section
D_v	vapour diffusivity
f	friction factor
F	fractional deposition
h	heat transfer coefficient
H	latent heat of vaporization
I	mean free path of air molecules
k	thermal conductivity of air
K_m	mass transfer coefficient
M_1	molecular mass (air)
M_2	molecular mass (moisture)
Q	rate of heat transfer
r	distance from tube centre
R	tube diameter
Re	Reynolds number
T	air temperature
u	radial component of velocity
$\bar{U}$	mean velocity
U^*	friction velocity
v	axial component of velocity
V_f	volumetric flow rate
V_1	deposition velocity
V_s	terminal velocity
V_{th}	velocity due to thermophoresis
u', v'	indicates a velocity fluctuation about a mean value.

Greek symbols

ρ_g	density of air
ρ_d	density of a droplet
σ_w	shear stress at wall
σ_g	size distribution parameter
μ	gas viscosity
τ	relaxation time
τ^+	scaled relaxation time.

flowed through a 1.5 m long entrance region, leading to the test-section.

The test-section (Fig. 3) was built around a 3 m long, 0.073 m internal diameter aluminium cylinder. Seven pairs of apertures were extruded for optical access, and a heating/cooling jacket was then fitted around this inner tube. Provision was made for traversing thermocouples along diameters at seven locations, and mounting thermocouples for surface temperature measurements (see Fig. 3 for locations). In addition, steel sample lines, leading to a dew point hygrometer, permitted determination of the air moisture content at inlet and outlet. A trap was milled into the base of the test section to collect deposit and condensate. (Note that throughout the rest of the paper, this position will be taken as the datum at which height = 0 m.)

A laser based device was used for simultaneous velocimetry and particle sizing (see Bates *et al.* [7]). This employed the principle of visibility for particle

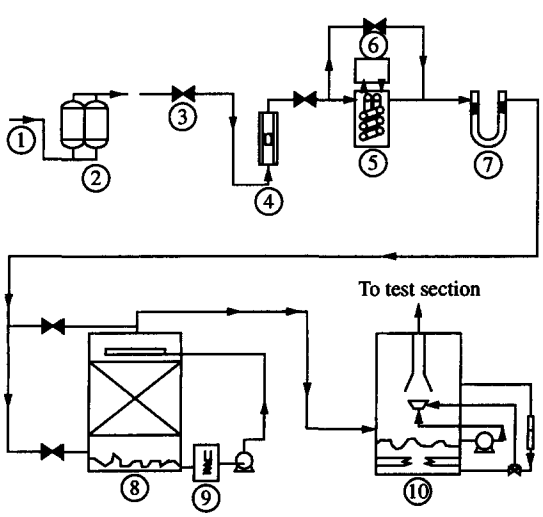

Fig. 1. Pre-treatment section. (1) Compressed air supply at 6 bar, (2) dryer, (3) regulating valve (to 1.1 bar), (4) rotameter, (5) heat exchanger (with by-pass), (6) glycol cooler (to −40°C), (7) electrical heater, (8) humidifying column (with by-pass), (9) electrical heater, (10) aerosol generator (see Fig. 2 for further details).

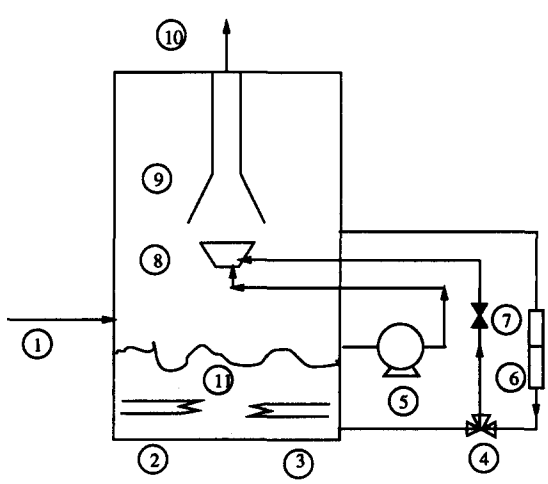

Fig. 2. Aerosol generator. (1) air supply, (2) electrical heater, (3) cooling coil (attached to glycol cooler), (4) three-way valve, (5) reciprocating compressor, (6) sight-tube, (7) needle valve, (8) nozzle, (9) tapered tube, (10) to test-section, (11) water reservoir.

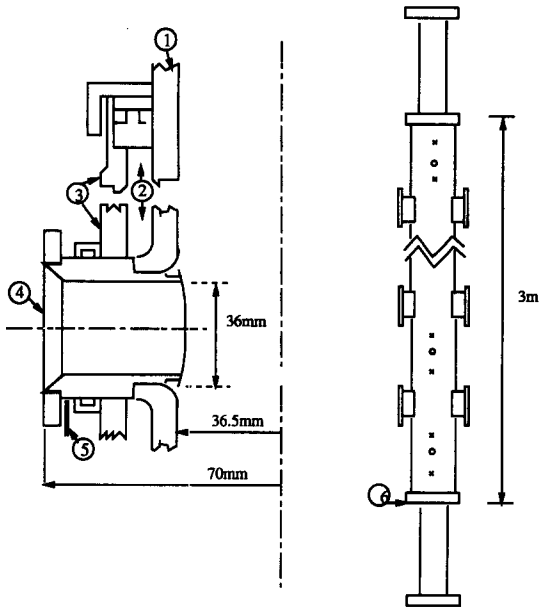

Fig. 3. The test-section. Part (a): cooling jacket seal plus optical window. Part (b): general arrangement. Part (a): (1) inner wall, (2) duct for coolant, (3) outer wall, (4) window, (5) drain tube. Part (b): X-location of thermocouple in inner wall. O-location of traversing probe. (6) entrance and datum position (height = 0 mm).

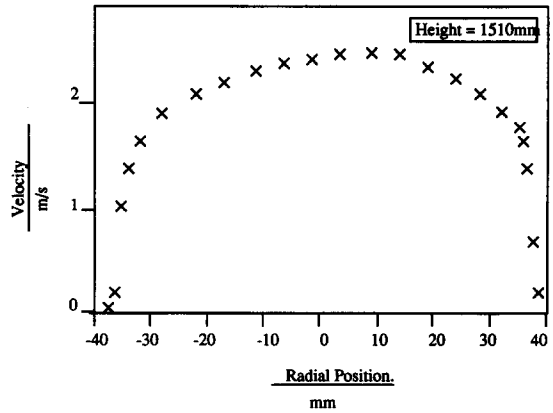

Fig. 4. Radial velocity profile.

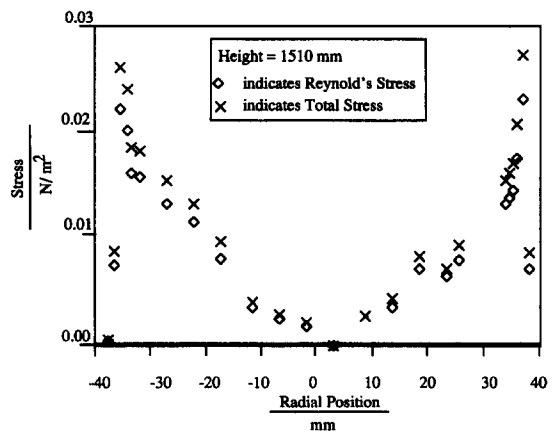

Fig. 5. Profile of shear stresses.

sizing, where particle size was correlated against a parameter characterising the shape of the doppler signal. (It has to be admitted that more recent, proprietary devices now tend towards phase doppler methods [8].)

A helium-neon laser and its associated optics produced concentric blue and green fringe patterns, with a spacing of 63 mm for the larger green pattern. The photomultipliers were offset from the lateral position by 9° with a collection angle of 10° to give the optimum resolution of particle diameter against visibility. It was this configuration that predetermined the necessary window size for the test-section.

PERFORMANCE OF THE TEST-SECTION

The hydrodynamic performance of the test-section was checked during a series of commissioning tests. This was in order to characterise the effects of the windows and the entrance region. We measured profiles of velocity and velocity fluctuation, wall shear stresses, and rates of heat transfer and condensation for comparison against correlations for developed flow in a smooth pipe.

Velocities were measured with a commercially available hot wire anemometry system, incorporating a Dantec type 55P53 cross wire probe. The alignment of the sensors was such that they were sensitive to $v+u$ and $v-u$ (v was the axial velocity component, and u the radial component). The 5 μm diameter wires were sufficiently fine to resolve velocity fluctuations greater than 30 kHz in frequency. Signal analysis and linearization was by analogue processing, to indicate mean values of u and v, and root mean square values of u', v', and $u'v'$.

The probe was traversed through the access windows at 1510 and 2890 mm above the test-section entrance. Velocity profiles did not extend significantly into the window recesses (see Fig. 4), and a second set of measurements with the probe held by hand confirmed that the values here were always less than 2% of the maximum flow velocity. Figure 5 shows the corresponding profile of shear stress, found from the sum of Reynolds and viscous components.

$$\sigma = \rho\overline{u'v'} + \mu\, \mathrm{d}\bar{v}/\mathrm{d}r \qquad (1)$$

The point of zero stress is 3 mm from the centre line, indicating a slight skewness in the flow.

The peaks in the measured stress near the positions flush with the tube walls were thought due to imperfections in the linearization of the signal, evident at lower velocities. In inferring friction factors we considered only measurements from positions more than 4 mm from the tube wall. From the extrapolated wall stresses:

$$f = 2\sigma_w/\rho_g v^2 \qquad (2)$$

Table 1. Inferred friction factors

Flow rate/ [1 min^{-1}]	Re	Friction factor at $y = -36.5$ mm	at $y = +36.5$ mm	Average	Blasius equation
		Height = 1510 *mm*			
310	6250	8.49×10^{-3}	9.77×10^{-3}	9.13×10^{-3}	8.88×10^{-3}
490	9720	9.14×10^{-3}	6.73×10^{-3}	7.94×10^{-3}	7.96×10^{-3}
640	12800	10.10×10^{-3}	6.98×10^{-3}	8.54×10^{-3}	7.43×10^{-3}
910	18100	11.80×10^{-3}	5.79×10^{-3}	8.80×10^{-3}	6.8×10^{-3}
		Height = 2890 *mm*			
460	9090	9.24×10^{-3}	7.00×10^{-3}	8.12×10^{-3}	8.09×10^{-3}
820	16360	12.00×10^{-3}	4.29×10^{-3}	8.15×10^{-3}	6.98×10^{-3}

which could be compared with values estimated from the Blasius equation for smooth tubes (see Table 1).

$$f = 0.079\, Re^{-0.25} \quad (2500 < Re < 10^5). \tag{3}$$

Friction factors were higher on one side than the other, confirming an asymmetry in the flow. The average values were similar to the accepted values for smooth tubes, particularly at the two lower flow rates.

Profiles of root mean square velocity fluctuation in the axial direction were also traversed (Fig. 6). These indicated turbulence intensities typically 15–20% higher than classical values [9].

To assess the heat transfer characteristics of the tube dry air was passed through the test-section with the side-walls cooled. Again, radial temperature profiles showed a small amount of skewness (Fig. 7).

Area weighted integration of measured profiles of temperature and velocity yielded the heat transfer by advection up the tube. The difference between values at the top and bottom of the test section was taken as the rate of heat transfer to the walls, Q. Using the log mean difference between mixing cup and side wall temperatures, a heat transfer coefficient was estimated:

$$h = \frac{Q/A}{(\Delta T)_{\mathrm{lm}}} \tag{4}$$

Nusselt and Reynolds numbers, based on tube diameter, are plotted on Fig. 8. Over the narrow range of conditions studied they compare moderately well with the Dittus–Boelter correlation of heat transfer, superimposed on the figure as a straight line.

Finally, the mass flux to the wall was inferred by the amount of condensate collected over a given time, and scaled to give a Sherwood number (Fig. 9). There is reasonable agreement with predictions based on the Chiltern–Colburn analogy between heat and mass transfer [10]. Note that dropwise rather than filmwise condensation had been observed: we assume that air was in contact with the wall, at the same temperature as the wall and saturated with vapour.

To summarize this section, we can state that average quantities (condensation rate, heat transfer, shear stress) were, over the narrow range of Reynolds numbers tested, reasonably close to the values expected in a smooth tube. There was, however, some skewness in measured velocity and temperature profiles. In principle, this might have been resolved by increasing the

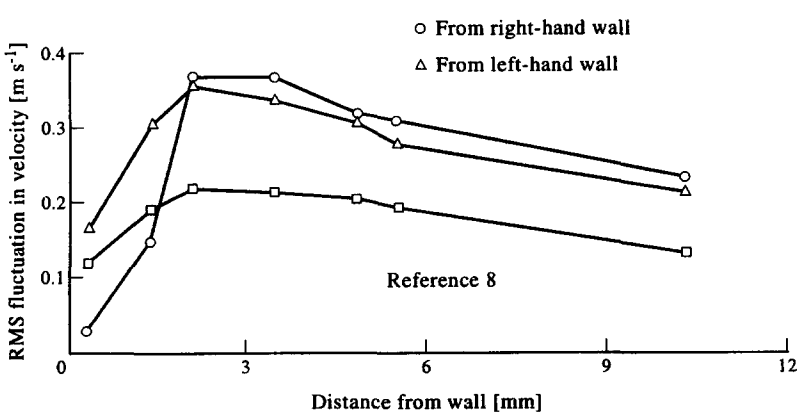

Fig. 6. Comparison of root mean square velocities (velocity fluctuations are in the usual direction).

length of the entrance region between the test-section and aerosol generator. Apart from the obvious implication of cost, this would have led to increased deposition within the entrance region.

PARTICLE DEPOSITION UNDER ADIABATIC CONDITIONS

Particle size distributions and deposition rates were measured over a variety of flow rates. To ensure adiabatic conditions, the cooling jacket was drained and the side-walls insulated. The relative humidity of the air component was increased as far as could be achieved in the pre-treatment section, and typically to 95%.

Measurement methods

The laser sizing system could be employed only for small droplet concentrations—typically 1 g m^{-3}. Denser aerosols would have saturated the measurement volume.

The log–normal distribution was used to describe samples of particle sizes, the appropriate parameters being the geometric mean diameter, d_g, and a parameter, σ_g, to represent the spread of the distribution.

$$d_g = \exp(\Sigma n_i \ln(d_i/\Sigma n_i) \quad (5)$$

$$\sigma_g = \exp((\Sigma(\ln(d_i) - \ln(d_g))^2/\Sigma n_i)^{1/2}. \quad (6)$$

Whilst d_g is a useful term with which to specify the size distribution, it tends to lend undue importance to smaller particles. A more appropriate mean diameter is calculated from the total mass of particles:

$$d_m = (\Sigma n_i d_i^3/\Sigma n_i)^{1/3}. \quad (7)$$

Deposition rates were assessed using a salt tracer. To allow sufficient particles to collect on the sides of the tube, a denser aerosol of about 10 g m^{-3} was necessary. The reservoir for the aerosol generator contained a weak, uniformly mixed salt solution (about 2 g l^{-1} of sodium chloride). The precise concentration was found by diluting a sample 20 times, and comparing its resistance against a calibration line (which was linear for concentrations less than 100 mg^{-1}). The rate of aerosol production was recorded by plotting the measured level in the aerosol generator against time.

At 30 min intervals the walls of the test-section were washed with 100 ml of distilled water, introduced at the top. On draining this would dissolve liquid present on the side walls, and collect in a trap at the test-section base. The salt content of the washings was inferred from their measured electrical conductivity. Thus the fractional deposition—or the proportion of droplets deposited in the duct—was:

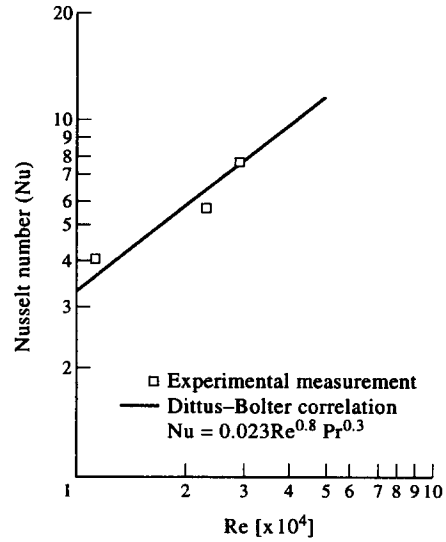

Fig. 8. Heat transfer performance.

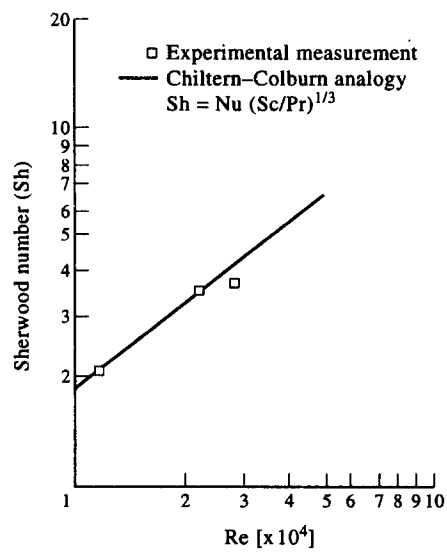

Fig. 9. Mass transfer performance.

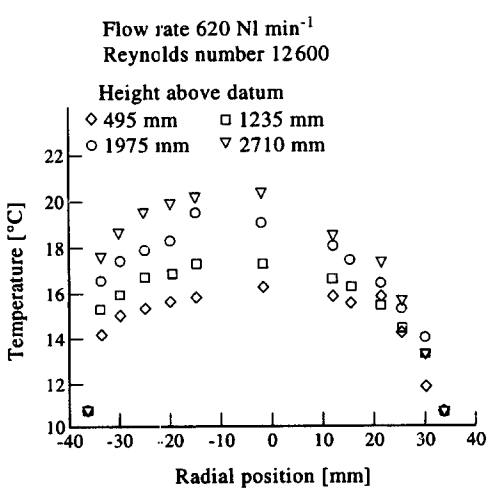

Fig. 7. Temperature profiles.

$$F = \frac{\text{mass of salt occurring in the washings per unit time}}{\text{mass of salt supplied in the aerosol per unit time}}. \tag{8}$$

Scaling procedures

It is desirable to report results in a scaled form, suitable for comparison against other reported work. We start with the definition of the 'relaxation time', τ, of a particle as a function of individual particle diameter and density, and gas viscosity:

$$\tau = \rho_p d_p^2 / 18\mu. \tag{9}$$

A non-dimensional form of τ is achieved with the friction velocity and kinematic viscosity:

$$\tau^+ = \tau U^{*2}/\nu \tag{10}$$

where U^* is related to the friction factor by:

$$U^* = (f/2)^{1/2}\bar{U}. \tag{11}$$

A deposition velocity is defined from the mass flux of particles from the gas stream to the side walls, and the mass concentration in the bulk:

$$V_1 = j_m/C. \tag{12}$$

V_1 can be deduced from the fractional deposition, using a differential component mass balance on the particles. The result is:

$$V_1 = \frac{(-V_f/A)}{\ln(1-F)}. \tag{13}$$

Scaling with the friction velocity gives:

$$V^+ = V_1/U^*. \tag{14}$$

Results for adiabatic conditions

A typical size distribution (Fig. 10), measured on the axis of the test-section and 1520 mm above its base, was characterized as: $d_g = 17\ \mu$m, $\sigma_g = 1.3$, and $d_m = 20\ \mu$m. The radial variation in d_g was small (Fig. 11).

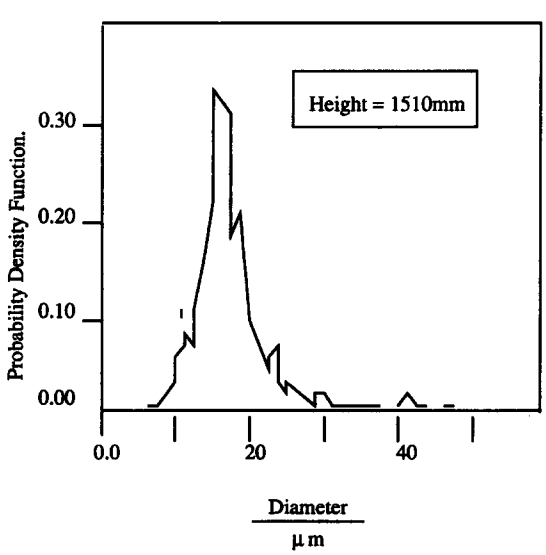

Fig. 10. A measured size distribution.

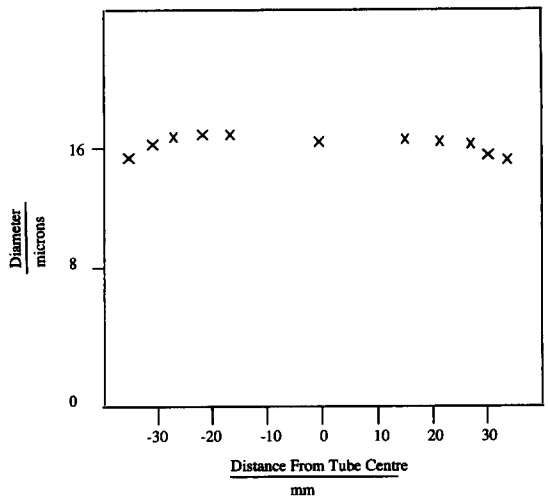

Fig. 11. Profile of mean droplet diameters.

Having established an estimate of particle diameter, plus a means of estimating deposition velocity, we were in a position to evaluate τ^+ and V^+. Note that in our work the relaxation time has been calculated from the mean diameter d_m, whereas most workers have used a monodisperse aerosol.

Flows were varied between 400 and 920 l min^{-1}, and the corresponding scaled parameters found (Fig. 12). The upper and lower limit's reported in Hanratty and McCoy's review [1] are sketched for comparison.

Discussion of results for adiabatic conditions

The deposition rates are at the upper limit reported in Hanratty and McCoy's review [1]. We can suggest two reasons for this: imperfections in the test-section, and the influence of size distribution.

Given the length of the entrance region (1.5 m or 20 pipe diameters), the flow was not fully developed in the lower part of the test-section. Moreover, skew-

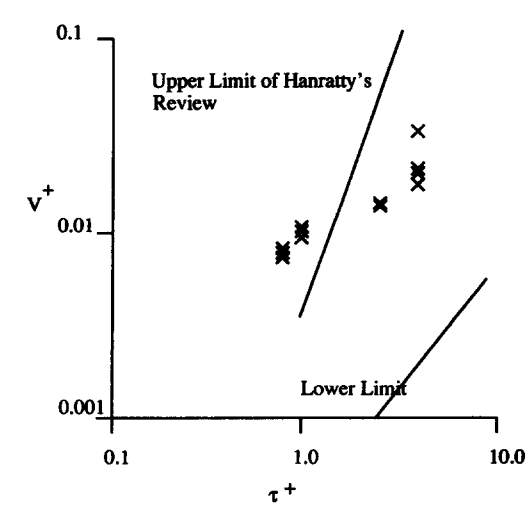

Fig. 12. Deposition rates for monodisperse particles.

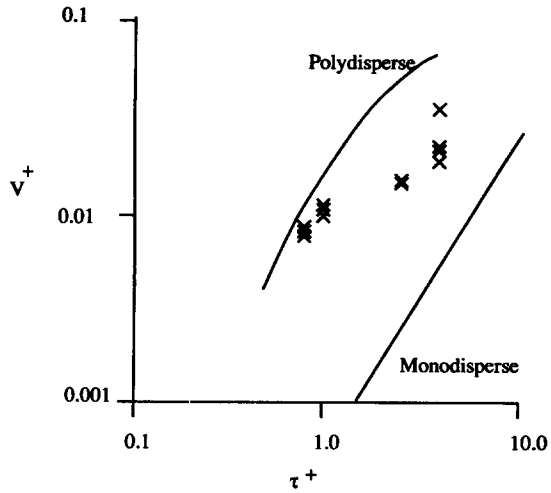

Fig. 13. Deposition rates for mono- and polydisperse particles.

ness in the flow pattern would have concentrated the particle deposition more on one side than the other.

With respect to size distribution, it is noted that most workers have used a near monodisperse aerosol, with σ_g no more than 1.1. For instance Lui and Agarwal [11] could guarantee the monodisperse condition by using a vibrating orifice particle generator. Within the eddy diffusivity–impaction regime ($1 < \tau^+ < 10$) their results correlate as:

$$V^+ = 0.6 \times 10^{-3}(\tau^+)^2 \quad (1 < \tau^+ < 10). \tag{15}$$

On Fig. 13, the lower curve is found simply by substituting d_m into the above equation. On the upper curve, a deposition velocity was estimated for each particle in the sample, and a weighted mean found:

$$V_1 = \Sigma(n_i d_i^3 V_{1,i})/\Sigma(n_i d_i^3). \tag{16}$$

The discrepancy between these two curves indicates the sensitivity of the predicted deposition rate to the nature of the size distribution.

It was necessary to check the consistency of size distribution between sparse and dense aerosol conditions. Theoretical work shows the effects of droplet evaporation to be small, provided that relative humidities are maintained above 95% [17]. The relative change in mean diameter is 4% for the sparse aerosol, and 2% for the dense aerosol.

PARTICLE DEPOSITION UNDER CONDENSATION CONDITIONS

For these experiments, the duct side walls were cooled to about 5°C, and the aerosol supplied at a range of temperatures. An aerosol density of about 10 g m^{-3} was supplied, with the relative humidity of the air component held at 95%. Results were compared against a phenomenological model.

Measurement methods

The particle size distribution was assumed to be that measured under adiabatic conditions. Again, the salt tracer method was used to infer the deposition velocity. However, the washing process was supplemented by typically 200 ml per hour of condensate. Preliminary tests, with the aerosol generator switched off, ensured that any condensate collected in the trap had a negligible electrical conductivity.

Given that the air was laden with droplets, exact measurement of the relative humidity within the test section was difficult with the equipment available. (The droplets would have destroyed the accuracy of any dew point hygrometer measurement.) Hence the condensation rate, R, was used to infer a mean concentration difference between the bulk air and the duct surface.

$$(\Delta C_v)_{lm} = \frac{R}{AK_m}. \tag{17}$$

The mass transfer coefficient, K_m, was estimated from the Chiltern–Colburn analogy.

The few available condensation measurements show the Chiltern–Colburn analogy to be good to within $\pm 5\%$ on average, within the range of Reynolds number discussed.

Prediction of deposition velocities

Predictions of deposition velocities were attempted with a calculation similar to that used by Byers and Calvert [12], who considered turbulence and thermophoresis effects for relatively small ($\sim$2 mm diameter) particles. The overall deposition velocity was estimated by summing these contributions along with that of diffusiophoresis.

The deposition velocities measured under adiabatic conditions were fitted to the following equation:

$$V^+ = V_1/U^* = 0.00773(\tau^+)^{0.758}. \tag{18}$$

In the presence of condensation there is a net movement of gas to a cooled surface, termed the 'Stefan flow'. For small mole fractions of vapour, this has a velocity:

$$V_s = (M_2/M_1)^{1/2} D(\mathrm{d}C_v/\mathrm{d}r)/\rho_g. \tag{19}$$

We have assumed that particles will achieve terminal velocity V_s in the diffusion sub-layers, at which position the gradient is, on average:

$$\mathrm{d}C_v/\mathrm{d}r = K_m(\Delta C_v)_{lm}/D_v. \tag{20}$$

Likewise, the greatest temperature difference is in the thermal boundary layers. For a Knudsen number less than 1, Davis [13] quotes the velocity due to thermophoresis as:

$$V_{th} = \frac{2.656k(T,p)\,\mathrm{d}T/\mathrm{d}Z}{pd_p} \tag{21}$$

where

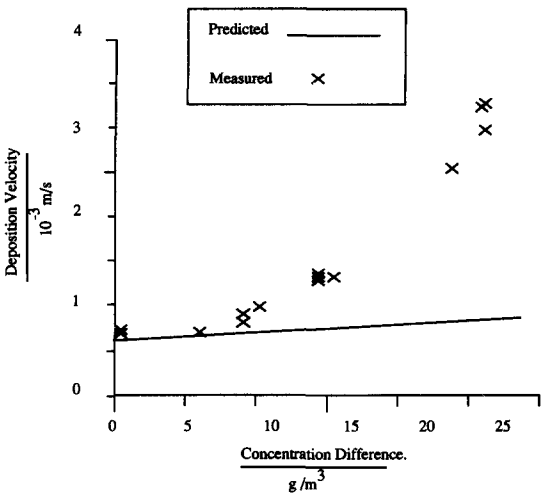

Fig. 14. Deposition rates under condensation conditions.

$$dT/dZ = h(DT)_{lm}/k. \quad (22)$$

Estimated and measured deposition velocities under condensation conditions

For a given flow rate, deposition velocities are clearly subject to concentration difference (Fig. 14). The trend is representative of data in Table 2, which includes flow rates between 420 and 920 l min^{-1}. The crude calculation listed above underpredicted the enhancement in deposition rate. The estimated influence of diffusiophoresis was an order of magnitude higher than thermophoresis (Table 3).

Discussion of predicted results

An application of some interest is deposition from sodium–argon aerosols, where droplet diameters of typically 2 μm are observed [14]. Hattori [15] has suggested that in this situation thermophoresis will dominate any diffusiophoresis effects. However, we point out that the Lewis number for gases is in the region of one, with the result that concentration and thermal sub-layers, in which both phoresis phenomena are most significant, will have a similar thickness, and hence a similar interaction with turbulence.

The straightforward addition of contributions to deposition velocity is a simplistic model of the interaction between turbulence and phoresis effects. However, we believe that a more complex analysis, accounting for transport through the full turbulence boundary layer, would not account fully for the large discrepancies between prediction and experiment.

The likeliest explanation is associated with surface roughness. Dropwise condensation occurred on the inner walls of the test-section, forming hemispheres of approximately 1 mm diameter. These could have increased the intensity of the air turbulence. In addition, they could have trapped aerosol, reducing the distance travelled through the boundary layers before the 'free flight' mechanism came into effect. Wood's theoretical work [3] indicates that this second effect can be important, even at roughnesses which would not affect the air turbulence.

Wood's gives theoretical estimates for the influence of roughness on a 'hydraulically smooth' regime. This

Table 3. Calculated deposition velocities

Component	Deposition velocity [m s^{-1}]
Turbulence	0.5308×10^{-3}
Thermophoresis	0.0249×10^{-3}
Diffusiophoresis	0.3735×10^{-3}
Total	0.9292×10^{-3}

Bulk temperature 30°C, wall temperature 5°C, droplet diameter 18 mm.

Table 2. Deposition rates measured under condensation conditions

Flow [l min^{-1}]	$(\Delta C)_{lm}$ [g m^{-3}]	Fractional deposition [%]	Deposition velocity [m s^{-1}]	τ^+	V^+
400	0.00	7.5	0.000773	0.88	0.00748
400	6.09	6.9	0.000692	0.88	0.00669
400	10.30	9.1	0.000946	0.88	0.00915
400	14.90	11.9	0.00125	0.88	0.0121
400	24.40	22.8	0.00255	0.88	0.0247
720	0.00	12.1	0.00229	2.46	0.0133
720	3.22	6.4	0.00118	2.46	0.00857
720	6.03	12.6	0.00239	2.46	0.0138
720	12.7	11.5	0.00217	2.46	0.0125
720	18.2	14.1	0.00272	2.46	0.0156
720	22.9	18.8	0.00371	2.46	0.0215
920	0.0	18.4	0.00462	3.78	0.0215
920	6.7	18.0	0.00452	3.78	0.0210
920	11.8	15.2	0.00376	3.78	0.0175
920	32.5	29.1	0.00783	3.78	0.0365

is restricted to a dimensionless roughness k^+ in the range 0–5, where:

$$k^+ = \frac{kU^*}{\nu}. \tag{23}$$

He explains the action of this roughness as reducing the necessary trajectory of particles under free flight. He gives curves for k^+ up to 4.2; these give qualitative agreement with the data of Montgomery and Corn [16].

Study of his predictions shows that at $\tau^+ = 2.46$, a value representative of our data, even roughnesses within the hydraulically smooth regime ($k^+ = 4.2$) lead to a six-fold deposition in turbulence effects. This alone would explain our discrepancy.

For a 1 mm droplet, we calculate $k^+ = 22$, a much greater value than, at first sight, is needed to explain our high deposition rates. However, it is difficult to relate roughness on surfaces such as sandpaper (used in classical friction factor studies) to the more sparsely distributed droplets.

What is required is a facility capable of 'freezing' droplets in position for surface analysis. This would permit better comparison of droplet size vs condensation rate, and permit further testing under adiabatic conditions. Such work is beyond the capabilities of the present system, but is under consideration for future studies.

Finally, we note that as particles were moved up the test-section, vapour would have condensed onto them, enlarging them and increasing the deposition velocity. Separate, theoretical work [17] shows that the increase in diameter would be 15% at most. Whilst there would have been some effect on deposition rate, it would have been small compared to the observed enhancement.

CONCLUSIONS

This paper has described a test-section manufactured for tests on the deposition rates of water–air aerosols, under a variety of thermal conditions. The hydrodynamics of the test-section were tested over a narrow range of Reynolds numbers, and some imperfections found. Whilst average friction factors, heat transfer coefficients and mass transfer coefficients were as expected, the flow was found to be skewed. In practice, this is a result of a compromise faced when first designing the experiment: too great an entrance region results in excess loss of particles by deposition, too little leads to under-developed flow.

The open literature reports wide variations in measured deposition rates, although the work of Lui and Agarwal [2] is most widely accepted. In applying a mean particle diameter to the analysis, our own results lie at the upper end of the previously reported data. Some error may well be due to the hydrodynamics of our test-section, but the influence of standard deviation in particle size on calculations is significant.

In the presence of condensation, deposition rates are enhanced markedly. Indeed, we cannot account for this even with liberal estimates of thermo- and diffusiophoresis effects. It is inferred that the roughening of the surface by dropwise condensation is responsible.

REFERENCES

1. H. Hanratty and D. McCoy, Review of particle deposition in circular ducts, *Int. J. Multiphase Flow* **3**, 319–331 (1977).
2. B. Lui and J. Agarwal, Experimental observations of aerosol deposition in turbulent flow, *J. Aerosol Sci.* **5**, 145–155 (1974).
3. N. Wood, A simple method for the calculation of turbulent deposition to smooth and rough surfaces, *J. Aerosol Sci.* **12**, 275–290 (1981).
4. T. Langrish and I. Zbicinski, The effects of air inlet geometry and spray cone angle on the wall deposition rate in spray driers, *Chem. Engng Res. Des.* **72**, 420–430 (1994).
5. K. Parkard and M. Choi, Conjugate heat transfer and particle deposition in the modified chemical vapour deposition process, *Int. J. Heat Mass Transfer* **37**, 1593–1606 (1994).
6. M. J. Dolias, Sodium aerosol development in an argon cover gas, in *4th Int. Conf. on Liquid Metal Engineering and Technology*, Vol. 1, pp. 113-1–113-11 (1988).
7. C. Bates, M. Yeoman, W. Roberts and W. Dalzell, Development of a laser system for simultaneous measurement of particle size and velocity AERE—Report R10210. Harwell Laboratory, Didcot, Oxon (1981).
8. M. Saffman, Optical particle sizing by phase-doppler anemometry, *Tech. Messen* **56**, 298–303 (1989).
9. P. S. Klebarof, NACA Technical Notes, 3178, Fig. 4 (1954).
10. A. Chapman, *Heat Transfer*, 3rd edn. Macmillan, New York (1974).
11. B. Lui and J. Agarwal, Construction of a vibrating orifice particle generator, *J. Aerosol Sci.* **6**, 123–131 (1975).
12. R. Byers and S. Calvert, Particle deposition from turbulent streams by means of thermal force, *Ind. Engng Chem. Fundam.* **8**, 855–866 (1969).
13. C. Davis, *Aerosol Science*. Academic Press, New York (1966).
14. G. Costigan and D. Roberts, Heat and mass transfer measurements from a hot sodium pool in an argon-filled enclosure, *10th Int. Heat Transfer Conf.* IChemE No. NR6 (1994).
15. N. Hattori, Paper issued at the *Int. Working Group on fast reactors*, Harwell Laboratory (1985).
16. T. L. Montgomery and M. Corn, Measurements of particle deposition on rough pipe surfaces, *J. Aerosol Sci.* **1**, 185–196 (1970).
17. M. Tierney and T. Bott, Prediction of aerosol development under evaporation conditions, in *14th Int. Conf. on Atmospheric Aerosols*, Vol. 4, pp. 581–585 (1996).